AD-A107 528 PENNSYLVANIA UNIV PHILADELPHIA F/G 20/8
STRUCTURE STUDY OF OXYGEN-ADSORBED NI(111) SURFACE BY HIGH ENER--ETC(U)
NOV 81 T NARUSAWA, W M GIBSON, E TOERNGRIST N00014-79-C-0991
UNCLASSIFIED TR-6 NL

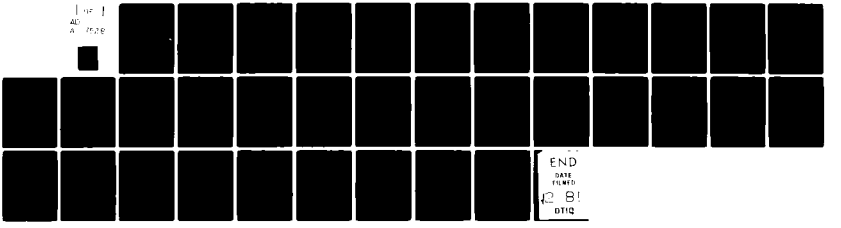

END
DATE FILMED
12 81
DTIC

UNCLASSIFIED

SECURITY CLASSIFICATION OF THIS PAGE (When Data Entered)

REPORT DOCUMENTATION PAGE	READ INSTRUCTIONS BEFORE COMPLETING FORM
1. REPORT NUMBER: Technical Report No. 6 — 2. GOVT ACCESSION NO: AD-A107 528	3. RECIPIENT'S CATALOG NUMBER:
4. TITLE (and Subtitle): STRUCTURE STUDY OF OXYGEN-ADSORBED Ni(111) SURFACE BY HIGH ENERGY ION SCATTERING (12)	5. TYPE OF REPORT & PERIOD COVERED: Interim
	6. PERFORMING ORG. REPORT NUMBER:
7. AUTHOR(s): T. Narusawa and W. M. Gibson Department of Physics, State University of New York at Albany, Albany, New York 12222 E. Törnqvist	8. CONTRACT OR GRANT NUMBER(s): N00014-79-C-0991
9. PERFORMING ORGANIZATION NAME AND ADDRESS: Trustees of the University of Pennsylvania Office of Project Research and Grants 3451 Walnut Street Philadelphia, PA 19104-3859	10. PROGRAM ELEMENT, PROJECT, TASK AREA & WORK UNIT NUMBERS: NR SRO-013/9-12-79 (472)
11. CONTROLLING OFFICE NAME AND ADDRESS: Office of Naval Research Department of the Navy 500 N. Quincy Street Arlington, VA 22217	12. REPORT DATE: November 4, 1981 13. NUMBER OF PAGES: 38
14. MONITORING AGENCY NAME & ADDRESS(if different from Controlling Office):	15. SECURITY CLASS. (of this report): Unclassified 15a. DECLASSIFICATION DOWNGRADING SCHEDULE

LEVEL II

16. DISTRIBUTION STATEMENT (of this Report)

Approved for public release; distribution unlimited

DTIC ELECTE NOV 19 1981 H

17. DISTRIBUTION STATEMENT (of the abstract entered in Block 20, if different from Report)

18. SUPPLEMENTARY NOTES

~~Preprint~~; accepted for publication in Surface Science

19. KEY WORDS (Continue on reverse side if necessary and identify by block number)

Nickel (111) surface; oxygen adsorption

20. ABSTRACT (Continue on reverse side if necessary and identify by block number)

Surface atomic structures of clean, oxygen-adsorbed, and oxidized (111) nickel have been studied quantitatively by using MeV ion scattering in combination with AES and MEED. We show that; the clean (111) nickel surface has the bulk-like structure with reconstruction or relaxation less than 0.02 Å, the surface thermal vibration amplitude is enhanced by ~20% compared to the bulk value, adsorbed oxygen results in surface lattice expansion by ~0.15 Å which is closely correlated to the p(2x2) or ($\sqrt{3}$x$\sqrt{3}$)R30° superstructure, and oxidation at room

(over)

DD FORM 1 JAN 73 1473 EDITION OF 1 NOV 65 IS OBSOLETE S/N 0102-014-6601

UNCLASSIFIED

SECURITY CLASSIFICATION OF THIS PAGE (When Data Entered)

AD A107528

DTIC FILE COPY

20. Abstract (continued)

temperature saturates at a stage which incorporates ~3 monolayers of nickel in a stoichiometric amorphous film of NiO whereas at temperatures higher than ~200°C thicker oxide films are produced. Our study indicates that each oxygen atom adsorbed on the Ni(111) surface interacts with and relaxes three nearest neighbor nickel atoms, and after saturation of the relaxation, oxidation of three monolayers takes place abruptly after which the oxide layer on the surface apparently blocks further reaction.

OFFICE OF NAVAL RESEARCH

Contract N00014-79-C-0991

Task No. NR SRO-013

TECHNICAL REPORT NO. 6

Structure Study of Oxygen-Adsorbed Ni(111) Surface by High Energy Ion Scattering

by

T. Narusawa, W. M. Gibson, and E. Törnqvist

Prepared for Publication

in

Surface Science

University of Pennsylvania
Office of Project Research and Grants
3451 Walnut Street
Philadelphia, Pennsylvania 19104-3859

4 November 1981

35

Accepted for Publication
in Surface Science Rec June 23, 1981

Structure Study of Oxygen-Adsorbed Ni(111) Surface by High Energy Ion Scattering

T.Narusawa and W.M.Gibson
Department of Physics
and
Institute for Particle Solid Interaction
State University of New York at Albany
Albany, New York 12222

and

E.Törnqvist
Department of Physics
and
Laboratory for Research on the Structure of Matter
University of Pennsylvania
Philadelphia, Pennsylvania 19104.

Abstract. Surface atomic structures of clean, oxygen-adsorbed, and oxidized (111) nickel have been studied quantitatively by using MeV ion scattering in combination with AES and MEED. We show that; the clean (111) nickel surface has the bulk-like structure with reconstruction or relaxation less than 0.02 Å, the surface thermal vibration amplitude is enhanced by ∿20 % compared to the bulk value, adsorbed oxygen results in surface lattice expansion by ∿0.15 Å which is closely correlated to the p(2x2) or $(\sqrt{3}x\sqrt{3})R30^{\circ}$ superstructure, and oxidation at room temperature saturates at a stage which incorporates ∿3 monolayers of nickel in a stoichiometric amorphous film of NiO whereas at temperatures higher than ∿200°C thicker oxide films are produced. Our study indicates that each oxygen atom adsorbed on the Ni(111) surface interacts with and relaxes three nearest neighbor nickel atoms, and after saturation of the relaxation, oxidation of three monolayers takes place abruptly after which the oxide layer on the surface apparently blocks further reaction.

1. Introduction.

The field of surface crystallography is still in its infancy. Accurate atomic positions are often not known even on rather simple-structured surfaces which show a bulk-like (1x1) diffraction pattern. The agreement between measurements and calculations of LEED I-V curves, which has been a major tool for surface structure investigation, is often unsatisfactory in uniquely defining the surface structure. The situation is even worse when the symmetry of the structure is lowered by reconstruction or adsorption-induced superstructures. Typically, for ordered species, the adsorbate binding site and its height over the substrate are used as model parameters for analysis of model structures using LEED data usually under an assumption of unstrained substrate surface structure. The success of this approach is often limited by the number of model structures that can be analyzed. On the other hand, there is growing evidence that the geometry of the substrate may be changed appreciably due to gas adsorption. In the particular case of Ni(111) surface, recent LEED measurements of temperature vs. coverage phase diagram for the O/Ni(111) system[1] and high resolution electron energy loss measurements for the H/Ni(111) system[2] have both suggested that the Ni(111) surface lattice might be reconstructed due to adsorption. We have presented definitive evidence of surface relaxation in the O/Ni(111) system by high energy ion scattering measurements[3].

In the present paper, we describe detailed experimental results of MeV He^+ ion scattering for the O/Ni(111) system, compare them to the results of computer simulation, and discuss possible structure models for the oxygen-induced p(2x2) and $(\sqrt{3}x\sqrt{3})R30^0$ superstructures and also the interface structure between the crystalline nickel substrate and the oxide overlayer. The usefulness of the so-called surface

peak intensity, which is measured in an aligned backscattering arrangement, has been well demonstrated elsewhere[4] as a structure-sensitive probe for surface studies. In addition, the ion scattering measurements combined with in-situ AES allows absolute oxygen coverage determinations over a wide range from submonolayer to over 10 monolayers coverage.

2. Experimental.

Clean Ni(111) surfaces were prepared in UHV by oxidation and reduction cycles and argon ion bombardment followed by annealing. Prolonged slow argon ion bombardment with the target at $\sim 600^{\circ}C$ was especially effective to remove the impurities carbon and sulfur which are common segregations on metal surfaces. The cleanliness and symmetry of the target surface were examined by in-situ AES and 5 keV electron diffraction (MEED). After the cleaning procedure, we measured a typical clean nickel Auger spectrum with no impurities exceeding 0.1 % in the surface atomic composition. The oxygen coverage in the initial stage of adsorption ($\lesssim 1$ monolayer = 1.86×10^{15} atoms/cm^2) was monitored by AES, whose absolute sensitivity was calibrated by ion backscattering measurements, and greater oxygen coverages ($\gtrsim 1$ monolayer) in the later adsorption or oxidation stage were measured directly by backscattering. In accordance with previous studies[1,5], we found two well developed superstructure diffraction patterns, p(2x2) and $(\sqrt{3}x\sqrt{3})R30^{\circ}$, in the course of oxygen adsorption at room temperature. The diffraction pattern gradually disappeared after the oxygen coverage of $\sim 1/3$ monolayers indicating the onset of amorphous oxide film formation.

The He^{+} ion beam of 0.5 to 2 MeV produced by SUNY-Dynamitron was introduced to the UHV target chamber through two 1 mm orifices. Scattered particles were analyzed by a Si detector of surface-barrier type, with an energy resolution of

~20 keV located in a grazing exit-angle geometry (~5° to the surface) to increase the surface sensitivity. The target orientation with respect to the incident beam was aligned in either the normal or non-normal axial channeling direction (see a marble model in Fig.1). Due to shadowing of the underlying atoms in a string by the surface atom, we can clearly isolate and evaluate the surface peak (SP) in the backscattering spectrum as shown in Fig.2. The oxygen peak intensity was evaluated after subtracting the Ni background, which was estimated by taking the average of the counts in each 10 channels on both sides of the oxygen signa Thus, we could determine the absolute oxygen coverage down to ~1 monolayer with an accuracy of ±15 %. The areal intensity of the SP was evaluated by using a standard background subtraction method[6] and compared to the random scattering yield to determine the number of backscattering Ni atoms (atoms/row).

In measurements of the angular distribution of the SP intensity, we obtained a series of spectra as shown representatively in Fig.3(a). We define the bulk yield and the surface yield as the integrated counts in the segments labelled "B" and "S", respectively, in the spectrum. If we plot these yields as a function of the incident angle we observe the familiar channeling dips as shown in Fig.3(b). The bulk yield shows a symmetric shape and its centroid can be used to locate the exact channeling direction (a <110> axis in the case of Fig.3). In contrast, the surface yield shows some asymmetric distribution which will be discussed in detail and related to the surface atomic structure. As shown in Fig.3(a), it gradually becomes harder to isolate the SP in the spectrum with increasing misalignment. Therefore, detailed spectral intensities were compared with calculation only within an angular range of ~±1 deg. from the axial channeling direction. We can still isolate the SP in this range, and we applied a similar background subtraction method as that described in ref.6 though this method becomes increasingly inaccurate with increasing minimum yield behind the SP as shown in spectra ② and ③ in Fig.3(a). The fluence of He^+ ion beam was ~1 $\mu C/mm^2$ (~6×10^{14} ions/cm^2) per each spectral measurement, which we determined to be far (≳2 orders)

~~below~~ below the critical value at which the effect of radiation damage or beam induced desorption becomes significant. The background pressure in the target chamber did not exceed 5×10^{-10} Torr during measurements.

3. Computer simulation.

The SP intensity of nickel was calculated by the nuclear encounter probability approach[7] assuming a number of surface atomic structure and dynamics models. Details of the calculation method have been discussed in the literature[5,7-9]. In brief, the paths of charged particles with given energy and direction, which impinge uniformly relative to a single string of target atoms, were traced in a stepwise manner by using a binary collision approximation. The consequent nuclear encounter probability for each atom in the string was summed to obtain the SP intensity.

The one-dimensional rms amplitude for bulk nickel atoms was calculated to be 0.068 Å assuming the target temperature of 300 ∿310 K during measurements and a bulk Debye temperature of 420 K. This value was used throughout the present study for the bulk amplitude, and the surface enhancement of thermal vibration was introduced through an exponential decay model similar to the calculation by Stensgaard et al[6], i.e. the enhancement was assumed to decay exponentially into the bulk with a decay constant of 3.52 Å (lattice constant of nickel). Possible anisotropy[9a] in the surface thermal vibration was not taken into account. We used a coefficient of 0.2 for the correlation of thermal vibration though an exact value for nickel is not known. Based on experimental phonon frequency distributions, Jackson et al[10,11] have calculated the correlation coefficients for Mo and Nb to

be between ∿0.2 and ∿0.3 at ∿300 K depending on the interatomic distance. These values are slightly lower than the Debye model prediction. We calculated the dependence of the SP intensity on the correlation coefficient and confirmed that the calculated result does not differ more than ±5 % if we choose a value between 0.1 and 0.3.

Shadowing of underlying nickel atoms by adsorbed oxygen was estimated using a similar method as that described in ref.9. The effect is maximized when the adsorbed oxygen sits exactly on top of the Ni string and decreases steeply with the misfit distance between the oxygen site and the string axis. In order to estimate the maximum effect, we assumed the 3-fold oxygen adsorption sites (A and B in Fig.1). The O-Ni distance was assumed to be (2.03+1.20) Å for site-A and (2x2.03+1.20) Å for site-B, where the distance of oxygen atom from the surface (1.20 Å) was that obtained from LEED analysis[12]. The results of simulation, however, is not very sensitive to this O-Ni distance[9]. The single string calculation for 1 MeV He^+ ions parallel to the <111> direction resulted in the shadowing effects of ∿0.17 atoms/row and ∿0.20 atoms/row for one monolayer of site-A and site-B oxygen, respectively. Since the oxygen coverage for the p(2x2) or $(\sqrt{3}x\sqrt{3})R30$ superstructure does not exceed ∿1/3 monolayers as will be discussed later, the net decrease of the SP intensity by the shadowing effect must be averaged and is therefore ∿1/3 or less of the single string calculation result , i.e. the shadowing effect by oxygen in the superstructures turns out to be ∿0.07 atoms/row at most. This is small enough to be neglected compared to the systematic error of measurements which we estimated to be ±5 %. If we assume the position of oxygen atom as described above, no shadowing effect is expected in the <110> incidence case because the oxygen atom is away from the <110> axis by ∿0.48 Å. We have earlier demonstarted that the shadowing effect from an amorphous overlayer is negligible[9]. The conclusion is that we can safely neglect the shadowing effect by adsorbed oxygen or amorphous oxide film in the following discussion.

In simulations of the angular scan of the SP intensity for oxygen adsorbed surfaces we have also used a single string approximation. This becomes inaccurate as the beam direction deviates from the channeling directions. We have previously found by using a multi-string simulation method[9] that small contributions from deeper atoms begin to be significant when the incident angle deviates more than about 1 deg. from the channeling direction. However, for deviation less than ±1 deg., the contribution from all atoms deeper than the 12th atom in a string sums up to less than 2 % of the total yield. Thus we can neglect the error due to the single string model within the angular range of ±1 deg. from the channeling direction.

4. Results and Discussion.

4.1 Clean surface.

The clean (1x1) surface shows a dependence of the SP intensity on incident He^+ ion energy as shown in Fig.4. Since our technique is sensitive to atomic displacements perpendicular to the incident direction, normal incidence measurements (a) give information about lateral, or in-plane, displacements of surface atoms, and non-normal incidence measurements (b) are sensitive to both lateral and longitudinal, or out of plane, displacements. The monotonic increase of the SP intensity in both figures corresponds to the decrease of shadowing effect with increasing incident energy and follows nicely the expected $E^{-1/2}$ dependence of the so-called shadow cone radius. Solid curves (a) and (b) in both figures are results of computer simulation. Both curves assume a bulk-like atomic structure,

and curve (a) assumes a bulk-like thermal vibration while curve (b) assumes a small enhancement (~20 %) in the surface thermal vibration amplitude. The agreement of curve (b) with the experimental plots in both figures, together with the (1x1) diffraction pattern, strongly suggests that the clean (111) nickel surface has the bulk termination structure. This agreement also suggests that anisotropy in the thermal vibration is small. In fact simulations indicate that anisotropy in the rms amplitude by as small as 0.004 Å should appear as a detectable variation in the SP intensity in the two different incident directions. This result is in reasonable agreement with Allen and de Wette[12a], who calculated the transverse and longitudinal enhancements in the mean square amplitude to be a factor of 1.30 and 1.86, respectively, in the high temperature limit approximation assuming force constants at the surface equal to those in the bulk. Enhancement of the surface thermal vibration assumed in curve (b) corresponds to a surface Debye temperature, θ_D, of about 330 K, which is in a good agreement with the LEED study[12] though another LEED study by Unertl cited in ref.9a suggests a lower value of ~150 K.

The symmetric angular distribution of the <110> SP intensity shown in Fig.5 confirms the above conclusion. Solid and dashed curves in this figure shows the results of computer simulation in which the bulk-like structure and an expansion of the first monolayer by 0.05 Å are assumed, respectively. The same enhanced surface thermal vibration as in Fig.4 is also assumed. The simulation result shows a significant asymmetry in the angular distribution even for relaxation of the first monolayer of only 0.02 Å. Consequently the observed symmetric distribution confirms that the surface structure is bulk-like. A slightly narrower distribution of the experimental plots compared to the solid curve suggests a possible higher vibrational amplitude hence lower value of θ_D than that used. Adoption of a value that fits the apparent width however leads to a too high value of the SP intensity in the aligned direction. We feel that the apparently narrower experimental distribution is a result of the larger uncertainty and probable insufficient magnitude of the background subtraction at the larger incidence angles.
However, there is no doubt about the symmetry of the angular distribution. We can conclude from this, from the agreement between the calculated and measured SP intensity in the vicinity of the <110> axis and from the energy dependence shown in Fig.4 that the clean (111) nickel surface has a bulk-like atomic structure

with relaxation or reconstruction less than 0.02 Å, and with ∿20 % nearly isotropic enhancement of surface thermal vibration amplitude. This results confirms the conclusion by LEED studies[12,13] in a straightforward and somewhat more quantitative manner.

4.2 Oxygen adsorption.

The SP intensities for <111> and <110> beam directions as a function of exposure of the crystal surface to O_2 gas at room temperature (300±5 K) are shown in Fig.6[3]. A striking difference between the two incident directions at low oxygen exposure indicates relaxation of surface atoms in a direction perpendicular to the surface. Also clear steps corresponding to superstructure MEED patterns as shown in the figure suggest that the relaxation is closely related to the superstructure. The absolute oxygen coverage measured at the exposures indicated by arrows in Fig.6 were 0.23±.04 monolayers for the ~~doubled~~ p(2x2) structure and 0.31±.05 monolayers for the $(\sqrt{3}x\sqrt{3})R30^0$ structure. The oxygen coverage increases to ∿0.36 monolayers at∿10 Langmuir exposure where an abrupt increase in the SP intensity occurs in both incident directions. This increase is accompanied with rapid disappearance of the MEED pattern, indicating the onset of amorphous oxide film formation. These results are consistent with LEED-AES studies[1,12]. The results shown in Fig.6 constitute a direct observation of surface relaxation of nickel substrate atoms connected with formation of the superstructures. However, since Fig.6 alone cannot lead us to a unique structure model, we analyzed the energy and angular dependences of the SP intensity in detail.

Figure 7 shows the energy dependence of the <110> SP intensity at the stage of the $(\sqrt{3}x\sqrt{3})R30^{\circ}$ structure. Solid curves were calculated assuming uniform relaxation of the first monolayer in the perpendicular direction to the surface by different amounts varying from 0.0 Å for the bottom curve to 0.52 Å for the top curve. Since the <110> direction is 35.26 deg. from the normal direction, these relaxations can be seen by the incident beam as displacements of the first atomic layer from the bulk lattice position from 0.0 Å to 0.30 Å in steps of 0.05 Å. The observed SP intensity lies close to or slightly below the third curve from the bottom. This suggests that the relaxation of the first monolayer is 0.15±.02 Å. In this measurement outward and inward relaxation play exactly the same role, so we cannot distinguish between expansion and contraction of the surface. Also the relaxation may not be restricted to the first monolayer since some combination of surface and/or subsurface strains would yield almost the same simulation result as shown in Fig.7.

Figure 8(a) and (b) compare the results of computer simulations with experimental angular scans of the <110> SP intensity for the p(2x2) and $(\sqrt{3}x\sqrt{3})R30^{\circ}$ structures, respectively. In the calculations we assumed uniform expansion of the first monolayer by various amounts as indicated for each curve in the figure. If contraction instead of expansion is assumed, the asymmetry and shift of the minimum point are reversed. This is not consistent with observation, so we can rule out surface contraction for both superstructures. In addition, since assumptions of relaxation in the second or subsurface layers do not yield proper angular distributions, we can essentially limit the relaxed atoms to the first layer.

The experimental plots in Fig.8(a) apparently agree with an expansion of $\sim$0.12 Å. On the other hand, the plots in Fig.8(b) are much closer to the simulation result

which assumes a uniform expansion of the first layer by 0.15 Å in a good agreement with the energy dependence shown in Fig.7. In order to further investigate the situation for the p(2x2) structure, we calculated some non-uniform expansion models as shown in Fig.9. The best fit is with curve (b) which assumes that 3/4 of the nickel atoms in the first monolayer are expanded by 0.15 Å and 1/4 are not expanded at all. Similar non-uniform expansion models[3] were also compared to the experimental plots for the $(\sqrt{3}x\sqrt{3})R30^0$ structure, however, in no case did we obtain better agreement than shown for the solid curve in Fig.8(b).

In the angular scan computer simulations we used the same enhanced thermal vibration model as determined in 4.1 for the clean surface. This approach is indicated by the constancy of the observed SP intensity with oxygen coverage up to ∿10 Langmuir for the <111> beam direction(Fig.6). Significant decrease in the thermal vibrational amplitude would result in decrease (or in the unlikely event of a vibration increase, in increase) in this direction, independent of relaxation of the surface layer.

All of our results taken together; that the oxygen coverage is ∿1/4 monolayers for the p(2x2) and ∿1/3 monolayers for the $(\sqrt{3}x\sqrt{3})R30^0$ structures, that 3/4 of the first monolayer is relaxed for the p(2x2) and all of the first monolayer is relaxed for the $(\sqrt{3}x\sqrt{3})R30^0$ structure and the LEED evidence that the 3-fold symmetry site is most likely for oxygen adsorption on (111) nickel surface leads to the atomic structure models shown in Fig.10 for the (1x1), p(2x2) and $(\sqrt{3}x\sqrt{3})R30^0$ structures. Oxygen atoms adsorbed on 3-fold sites (site-B in Fig.1) are shown by large shadowed circles, and small closed and open circles represent the expanded and non-expanded (bulk-like) nickel atoms in the first monolayer, respectively. Neither the LEED nor ion scattering results differentiate between the A or B adsorption sites. For both

structures only one type of site is occupied-perhaps electronic structure calculations can be used to identify the lowest energy of the two possible configurations. The transition from the p(2x2) to the $(\sqrt{3}x\sqrt{3})R30^0$ structure in this model involves motion of 1/2 of the oxygen atoms to other bonding sites. Formation of the p(2x2) structure over the entire surface before the phase change to the $(\sqrt{3}x\sqrt{3})R30^0$ structure implies that it is a lower energy configuration than islands of the $(\sqrt{3}x\sqrt{3})R30^0$ structure. In any case our atomic model suggests the Ni_3O cluster as an electronically stable composition on the oxygen adsorbed (111) nickel surface.

4.3 Oxidation.

When the crystal surface is exposed to O_2 gas at room temperature both of the <111> and <110> SP intensities increase abruptly at an exposure of ∿10 Langmuir, where the oxygen coverage was measured to be ∿0.36 monolayers. The increase in the SP intensities apparently saturates after an exposure of about 100 Langmuir as shown in Fig.6. The saturation increase is ∿1 atoms/row for the <111> SP intensity and ∿3 atoms/row for the <110> SP intensity. Since the incident beam sees directly top three monolayers in a <111> direction and only the first monolayer in the <110> incident direction, both of these saturation increases correspond to release of the first three monolayers of nickel atoms from registration with the lattice. In detail this result shows that the first three monolayers are displaced an amount large compared to the shadow cone radius at 2 MeV (∿0.06 Å in the <110> incidence and ∿0.1 Å in the <111> incidence) and are not correlated with each other. This, together with the disappearance of the MEED pattern at this stage, suggests an amorphous oxide layer formation. Measurements of the angular distribution of the nickel and oxygen scattering intensity support this conclusion. Figure 11 shows the energy dependence of the SP intensity for the oxygen saturated surface at

room temperature. We can derive some information about the interface atomic structure form these measurements by using the concept of the shadow cone radius. Figure 11(b) shows that the difference between the "clean" and "oxygen saturated" SP intensities is ∿3 atoms/row for <110> incidence over the whole energy range studied, which confirms large displacements of the first three monolayers. On the other hand, Fig.11(a) shows that the similar difference in the <111> incidence case is ∿1 atom/row in the high energy range but decreases to ∿0.7 atoms/row in the low energy range. The shadow cone radii at 0.6 MeV at the position of the second atom in each row are ∿0.116 Å for <110> incidence and ∿0.181 Å for <111> incidence. Therefore, Fig.11(a) and (b) indicate that displacements of the nickel in the top three layers are well above ∿0.12 Å in a direction perpendicular to the <110> direction. However, the displacements of some of the atoms in the three layers, probably the layer nearest the interface, are ≲0.18 Å when viewed in the direction normal to the surface. This suggests that the oxide overlayer is not really amorphous throughout but some registration still exists to the underlying crystal, whose structure is not distorted within the accuracy of the measurement (∿0.05 Å).

The absolute oxygen coverage measurement at the saturation stage resulted in 2.8±.4 monolayers confirming formation of ∿3 monolayers of oxide film giving a stoichiometry of NiO. This agrees fairly well with a nuclear microanalysis measurements by Norton et al[13a], however, it disagrees with LEED-AES measurements[14] which concluded the saturation coverage to be 1.6 layers of NiO at room temperature. We believe this disagreement is due to the difficulty of AES in performing absolute coverage measurements, especially in a range thicker than 1 monolayer. Previous studies of the oxidation of the nickel surface using LEED-AES[14] and ion scattering[15] have concluded that the saturation thickness is ∿2 monolayers for both the (100) and (110) surfaces, respectively. If this is true,

it is interesting to note that both of these surfaces expose the top two layers directly to the vacuum.

4.4 High temperature measurements.

When the crystal was kept at temperatures higher than ∿350 K and less than ∿470 K during the oxygen exposure and measurements, we could discern a weak diffraction pattern corresponding to the p(2x2) structure in the initial stage of oxygen adsorption, but the $(\sqrt{3}x\sqrt{3})R30^0$ structure was not detected. Neither of these structures were found if the crystal temperature exceeded ∿470 K. Instead, we found a diffuse and streaky diffraction feature after an exposure of ∿10 L, which seemed to become sharper and stronger with increased oxygen exposure and increased crystal temperature which indicates crystalization of the NiO film. These MEED results are in a good agreement with previous LEED studies[1,14].

Variation of the <110> SP intensity is shown in Fig.12 for 420 K and 520 K measurements. The SP intensity for 2 MeV ions for the clean surface at these temperatures were 4.32 and 4.48 atoms/row, respectively. The difference between these values and that at room temperature shown in Fig.4(b) is due to the increase in the thermal vibration and agrees well with computer simulations. In case of 420 K measurements, the initial increase in the SP intensity in the exposure region lower than ∿10 L is about the same as that corresponding to the p(2x2) structure in Fig.6. Although detailed angular or energy distribution measurements have not been carried out, the surface strucutre is probably similar to that shown in Fig.10. As observed for lower temperature measurements the SP intensity

increases at aroud 10 L. However, the oxygen coverage at 10 L was measured at ∿0.31 monolayers (vs. ∿0.36 monolayers at room temperature) and the rate of increase in the SP intensity is lower than at room temperature. We believe these differences arise from a lower sticking probability of oxygen on the (111) surface at the high temperature. The apparent saturation level at 420 K is ∿3 atoms/row which agrees with room temperature measurements. At 520 K, the initial increase in the SP intensity is slightly higher than the room temperature or 420 K measurements. This, together with no diffraction feature observed at this temperature, is consistent with the suggestion from LEED and ion scattering studies[14,15] that adsorbed oxygen reacts with nickel and makes small clusters of NiO. The possible intermediate decrease in the SP intensity at ∿8 L may be explained by agglomeration of small clusters to larger islands. Increase of the SP intensity after ∿10 L exposure is also slow in this case but continues without saturation. We have measured up to an exposure of 900 L where the increase of SP intensity was ∿16 atoms/row, which indicates oxide film formation involving more than ∿16 monolayers of nickel. The rate of increase shows a tendency to decrease with increasing thickness suggesting that the oxidation may be limited by diffusion. Although comparison of aligned and random spectra in this stage showed a significant difference in the nickel and oxygen peak intensity indicating crystalline structure of the oxide film, the ratio of the aligned peak intensity to the random (∿80 %) is evidence of considerable disorder in the film. The temperature dependence of the oxidation presented here is in a good agreement with previous studies.

5. Summary.

We have applied high energy ion scattering to a study of clean, oxygen-adsorbed, and oxidized (111) surface of nickel and shown that;

1) The clean surface has the bulk-like structure with relaxation or reconstruction less than $\sim$0.02 Å.
2) The surface thermal vibration of the clean surface is enhanced by $\sim$20 % compared to the bulk.
3) The p(2x2) structure induced by adsorption of $\sim$1/4 monolayers of oxygen is accompanied by outward relaxation (lattice expansion) of $\sim$3/4 of the nickel atoms in the first monclayer by $\sim$0.15 Å perpendicular to the surface.
4) The $(\sqrt{3}x\sqrt{3})R30^0$ structure induced by adsorption of $\sim$1/3 monolayers of oxygen is accompanied by outward relaxation of all of the atoms in the first monolayer of the nickel crystal by $\sim$0.15 Å.
5) Oxidation of the (111) nickel surface takes place at $\sim$0.36 monolayers coverage at room temperature and at slightly lower coverage at higher temperatures.
6) Saturation of the oxide film thickness involves $\sim$3 monolayers of nickel at temperatures lower than $\sim$470 K. At higher temperatures there is no saturation in the exposure range studied.
7) The oxide composition is NiO. It is amorphous with some indication of registration at the interface with the substrate crystal at room temperature, and crystalline at higher temperatures.
8) The interface structure is very sharp with distortion of the substrate lattice less than $\sim$0.05 Å at room temperature.

These results are consistent with previous studies [redacted] and provide complementary new information on the surface structure. A detailed interface study of the epitaxial system such as NiO/Ni(111) presented here briefly is an interesting topic for high energy ion scattering, however, it is beyond the scope of this paper.

Acknowledgement is due to L.C.Feldman, Bell Telephone Laboratories, and T.Gustaffson and E.W.Plummer, University of Pennsylvania, for invaluable suggestions and stimulating discussions. This work was supported by the Office of Naval Research under Contract No.N00014-78-C-0616. One of us (ET) acknowledges the support from the Office of Naval Research under Contract No.N00014-79-C-0991.

References.

1) L.D.Roelofs, A.R.Kortan, T.L.Einstein and R.L.Park; ~~to be published~~ in J.Vac.Sci.Technol. 18 (1981) 492.

2) W.Ho, N.J.DiNardo and E.W.Plummer; J.Vac.Sci.Technol. 17 (1980) 134.

3) T.Narusawa, W.M.Gibson and E.Törnqvist; Phys. Rev. Letters 47 (1981) 417.

4) E.Bogh in Channeling: Theory, Observation and Applications, ed. by D.V.Morgan, John Wiley & Sons, New York (1973).

L.C.Feldman in Surface Science: Recent Progress and Perspectives, ed. by R.Vanselow, CRC Press, Ohio (1980).

5) H.Ibach and D.Bruchmann; Phys.Rev.Letters 44 (1980) 36.

6) I.Stensgaard, L.C.Feldman and P.J.Silverman; Surface Sci. 77 (1978) 513.

7) J.H.Barrett; Phys.Rev. B3 (1971) 1527.

8) S.T.Picraux, W.L.Brown and W.M.Gibson; Phys.Rev. B6 (1972) 1382.

9) K.Kinoshita, T.Narusawa and W.M.Gibson; Surface Sci. 110 (1981) 334.

9a) M.G.Lagally, in Surface Physics of Materials, vol.2, ed. J.M.Blakely, Academic (1975) p419.

10) D.P.Jackson, B.M.Powell and G.Dolling; Phys.Letters 51A (1975) 87.

11) D.P.Jackson and J.H.Barrett; Comput. Phys. Commun. 13 (1977) 157.

12) P.M.Marcus, J.E.Demuth and D.W.Jepsen; Surface Sci. 53 (1975) 501.

12a) R.E.Allen and F.W.de Wette; Phys. Rev. 188 (1969) 1320.

13) J.E.Demuth, P.M.Marcus and D.W.Jepsen; Phys.Rev. B15 (1975) 1460.

13a) P.R.Norton, R.L.Tapping and J.W.Goodale; Surface Sci. 65 (1977) 13.

14) P.H.Holloway and J.B.Hudson; Surface Sci. 43 (1974) 123, 141.

15) R.G.Smeenk, R.M.Tromp, J.F.Van der Veen and F.W.Saris; Surface Sci. 95 (1980) 156.

Figure Captions.

Fig.1 Marble model of bulk-like Ni(111) surface atomic structure.
Circles of different sizes correspond to atoms in different planes. The large, medium, and small circles in the top view represent the atoms in the first, second, and third layers, respectively. The side view shows {110} planes perpendicular to the surface. Note the incident beam in the <111> channeling direction sees top three monolayers whereas only the first monolayer in the <110> or <100> direction. A and B in the top view show two different kinds of 3-fold symmetry sites for oxygen adsorption.

Fig.2 Typical aligned backscattering spectra from clean and oxygen adsorbed Ni(111) surfaces.
He^+ ion beam; 0.6 MeV, 0.4 μC and <110> incidence. The exposure to O_2 gas is 100 L (1 L = $1x10^{-6}$ Torr·sec) at room temperature for the upper spectrum.

Fig.3 Angular dependence of backscattering spectrum (a), and bulk and surface yields (b).
The incident He^+ ion beam is at 1 MeV and in the vicinity of the <110> direction in the {110} plane. The bulk and surface yields are defined as the integrated counts in the segments labelled "B" and "S" in (a), and plotted in closed and open circles in (b), respectively. Circled numbers in (a) and (b) correspond to each other and show angular setting of the crystal with respect to the incident beam. Data were taken for the $(\sqrt{3}x\sqrt{3})R30^\circ$ structure.

Fig.4 Energy dependence of surface peak intensity for clean Ni(111)-(1x1) structure.

(a): <111> incidence, (b): <110> incidence. The uncertainty of absolute measurements (±5 %) are shown by error bars. Solid curves in both figures are the results of computer simulations. Simulation (a) assumes a bulk-like structure and isotropic bulk-like thermal vibration, i.e. one-dimensional rms amplitude of 0.068 Å. Simulation (b) assumes a bulk-like structure and an enhanced surface thermal vibration, i.e. one-dimensional rms amplitude of 0.084 Å for the first layer, 0.077 Å for the second layer, 0.072 Å for the third layer, and 0.068 Å for the fourth and underlying layers.

Fig.5 Angular dependence of <110> surface peak intensity at 1 MeV for clean Ni(111)-(1x1) structure.

The uncertainty of relative measurements, shown by the error bars, was estimated to be ±3 % and ±6 % near the centroid and the peripheries of the distribution, respectively. Solid and dashed curves show the results of computer simulations in which a bulk-like structure and a uniform expansion of the first layer by 0.05 Å are assumed, respectively.

Fig.6 Variation of <111> and <110> surface peak intensities at 2 MeV as a function of exposure to oxygen. Room temperature measurements.

Exposures which give most intense superstructure diffraction patterns are inducated by arrows. Error bars are for ±3 % for relative SP intensity measurements and ±10 % for oxygen exposure measurements.

Fig.7 Energy dependence of <110> surface peak intensity for Ni(111)-$(\sqrt{3}x\sqrt{3})R30^{\circ}$-O structure.

Simulation curves assume uniform relaxation of the first monolayer in the direction perpendicular to the surface by various amounts indicated in the figure. The same enhanced thermal vibration model as in Fig.4 is assumed.

Fig.8 Angular dependence of <110> surface peak intensity at 1 MeV for (a) Ni(111)-p(2x2)-O structure and (b) Ni(111)-($\sqrt{3}$x$\sqrt{3}$)R30°-O structure. Simulation curves assume the enhanced surface thermal vibration (fig.4) and uniform expansion of the first monolayer in the direction perpendicular to the surface by various amounts indicated in the figure. The exact <110> direction was determined from simultaneous measurements of the bulk yield.

Fig.9 Angular dependence of <110> surface peak intensity at 1 MeV for Ni(111)-p(2x2)-O structure compared to simulations of non-uniform surface expansion models. Simulation (a) assumes the expansion of all nickel atoms in the first monolayer by 0.15 Å (same as Fig.8(a)). Simulation (b), (c), and (d) assume that 3/4, 1/2, and 1/4 of the nickel atoms in the first monolayer are expanded by 0.15 Å, respectively, and the remainder are not relaxed at all. The enhanced surface thermal vibration is assumed.

Fig.10 Atomic structure models for Ni(111)-(1x1), -p(2x2)-O, and -($\sqrt{3}$x$\sqrt{3}$)R30°-O structures.

Large shadowed circles represent oxygen atoms adsorbed on 3-fold symmetry sites (site-B in Fig.1). Small closed and open circles represent the expanded and non-expanded nickel atoms in the first monolayer, respectively.

The second and underlying layers are bulk-like (not shown in the figure).

Fig.11 Energy dependence of (a) <111> and (b) <110> surface peak intensities for oxygen-saturated Ni(111) surface at room temperature. Experimental results for the clean surface are also shown for comparison. Solid curves are just visual fits. Exposure to oxygen:100 L.

Fig.12 Variation of <110> surface peak intensity at 2 MeV as a function of exposure to oxygen. 420 K (open circles) and 520 K (closed circles) measurements. Increase of the SP intensity by 1 atom/row corresponds to displacements of one monolayer in the first-order approximation for <110> incidence.

Ni (111)

Top View

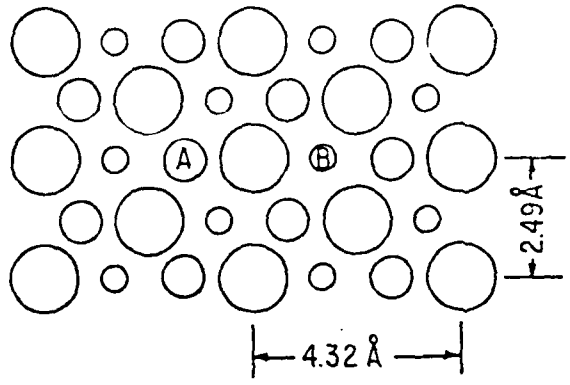

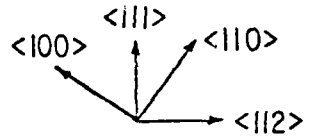

Side View

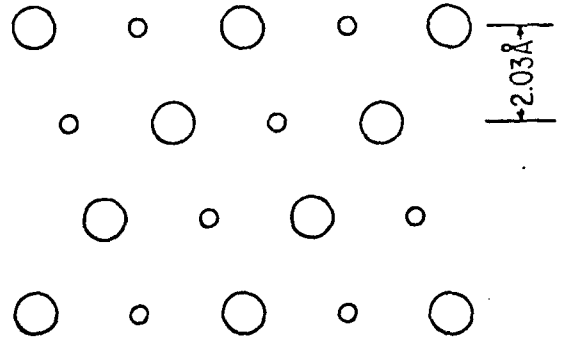

Fig 1

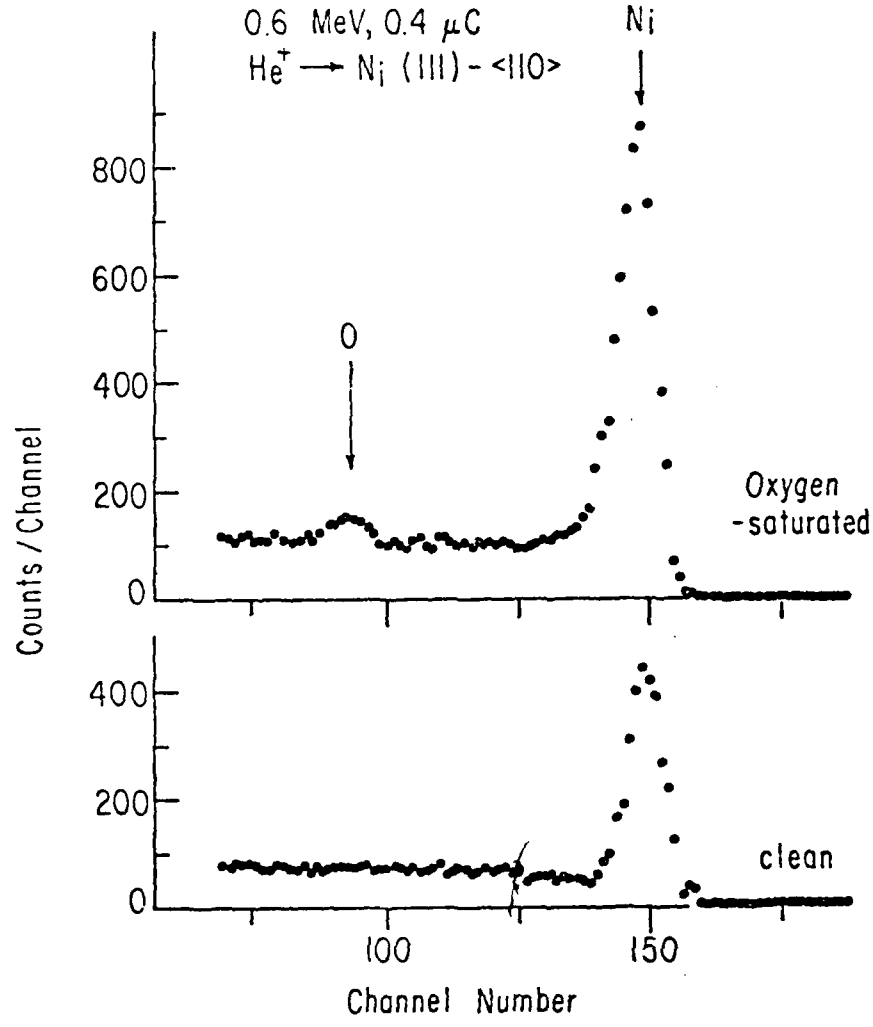

Fig 2

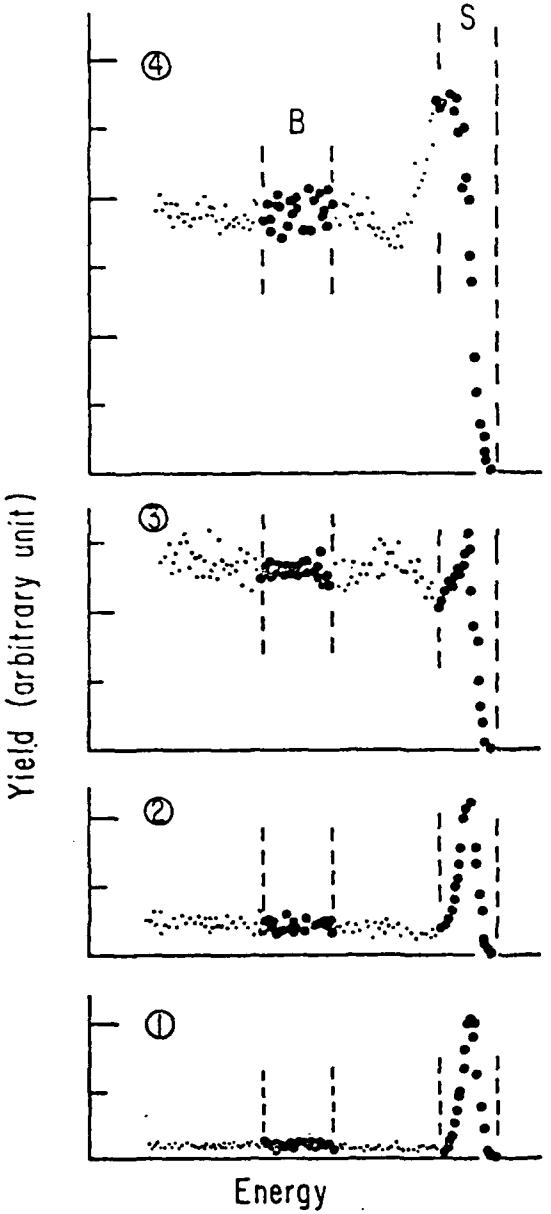
S
④
B
③
②
①
Yield (arbitrary unit)
Energy

Fig. 3 (a)

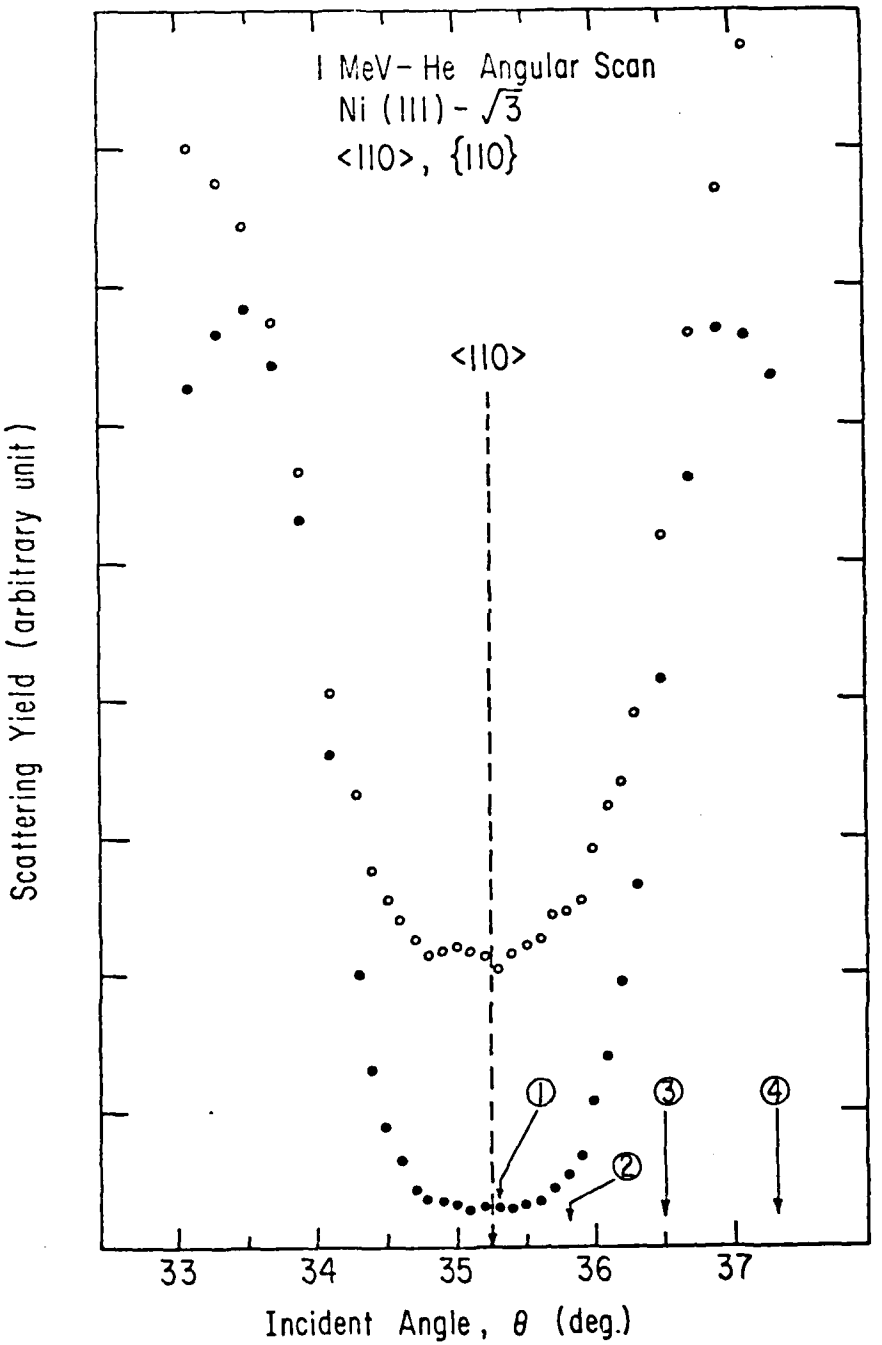
1 MeV - He Angular Scan
Ni (111) - √3
<110>, {110}
<110>
①
②
③
④
Scattering Yield (arbitrary unit)
33
34
35
36
37
Incident Angle, θ (deg.)

Fig 3(b)

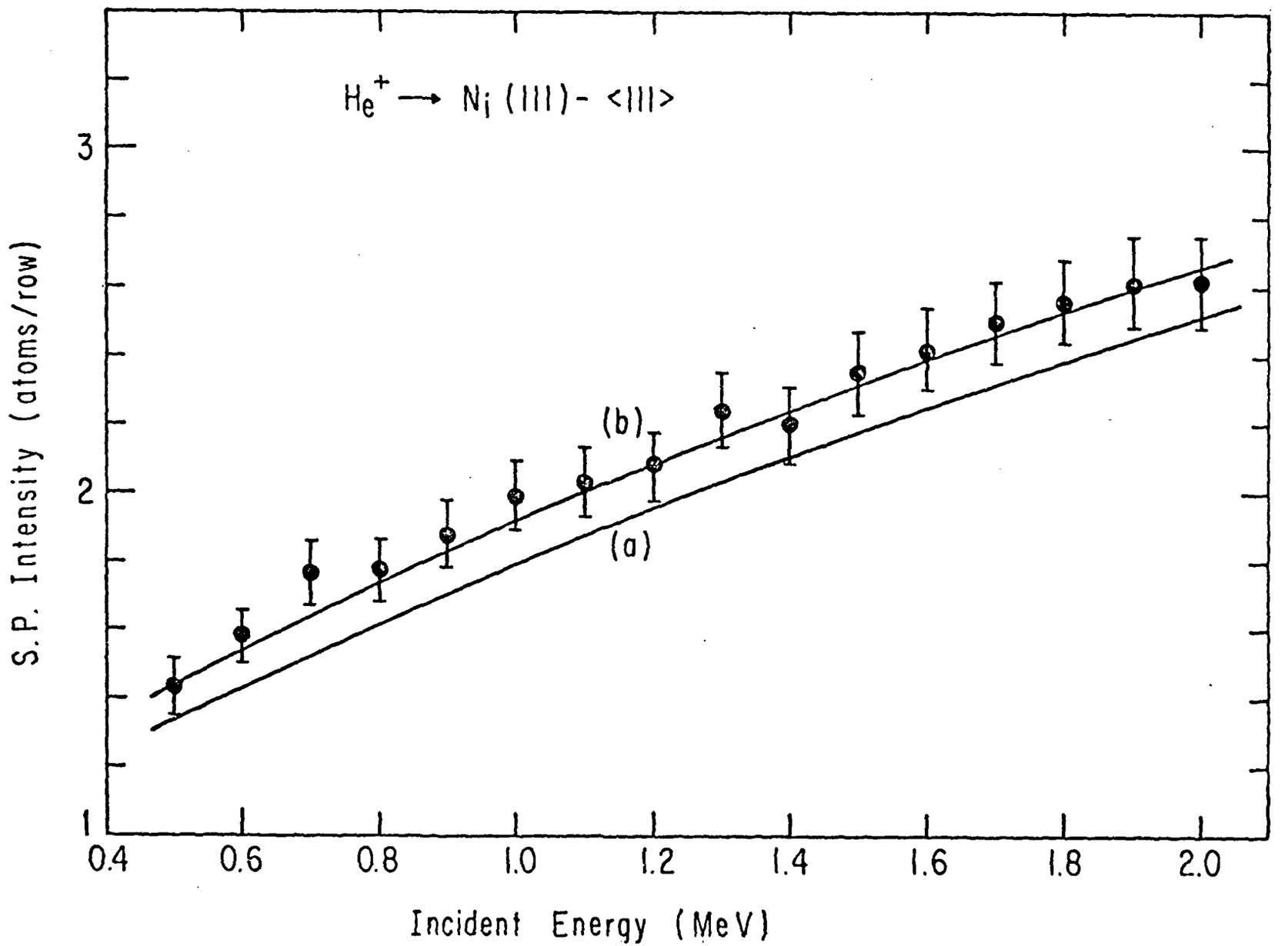
$He^+ \rightarrow Ni\ (111) - \langle 111 \rangle$
S.P. Intensity (atoms/row)
3
2
1
0.4
0.6
0.8
1.0
1.2
1.4
1.6
1.8
2.0
Incident Energy (MeV)
(b)
(a)

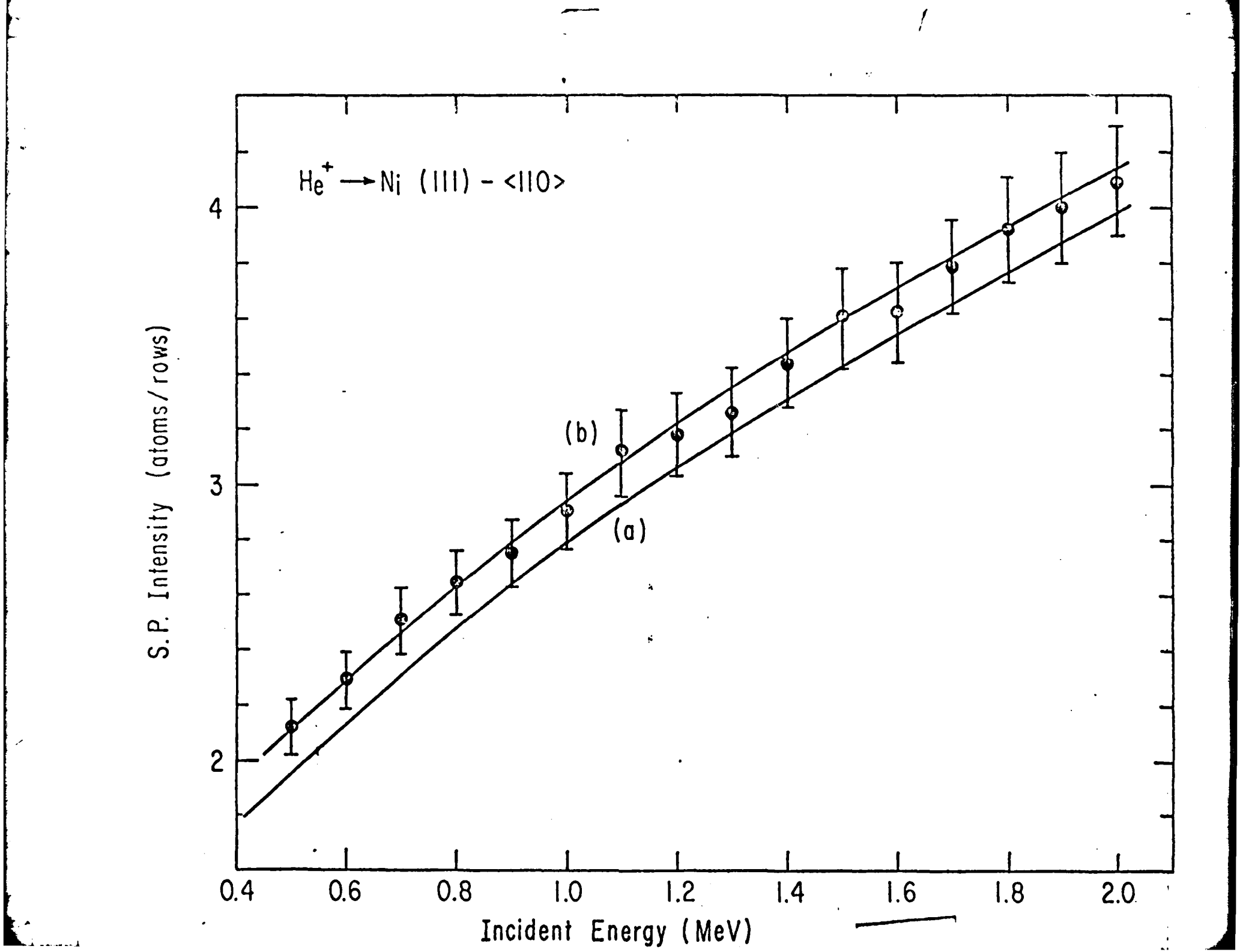
$He^+ \rightarrow Ni\ (111) - \langle 110 \rangle$
S.P. Intensity (atoms/rows)
4
3
2
(b)
(a)
0.4
0.6
0.8
1.0
1.2
1.4
1.6
1.8
2.0
Incident Energy (MeV)

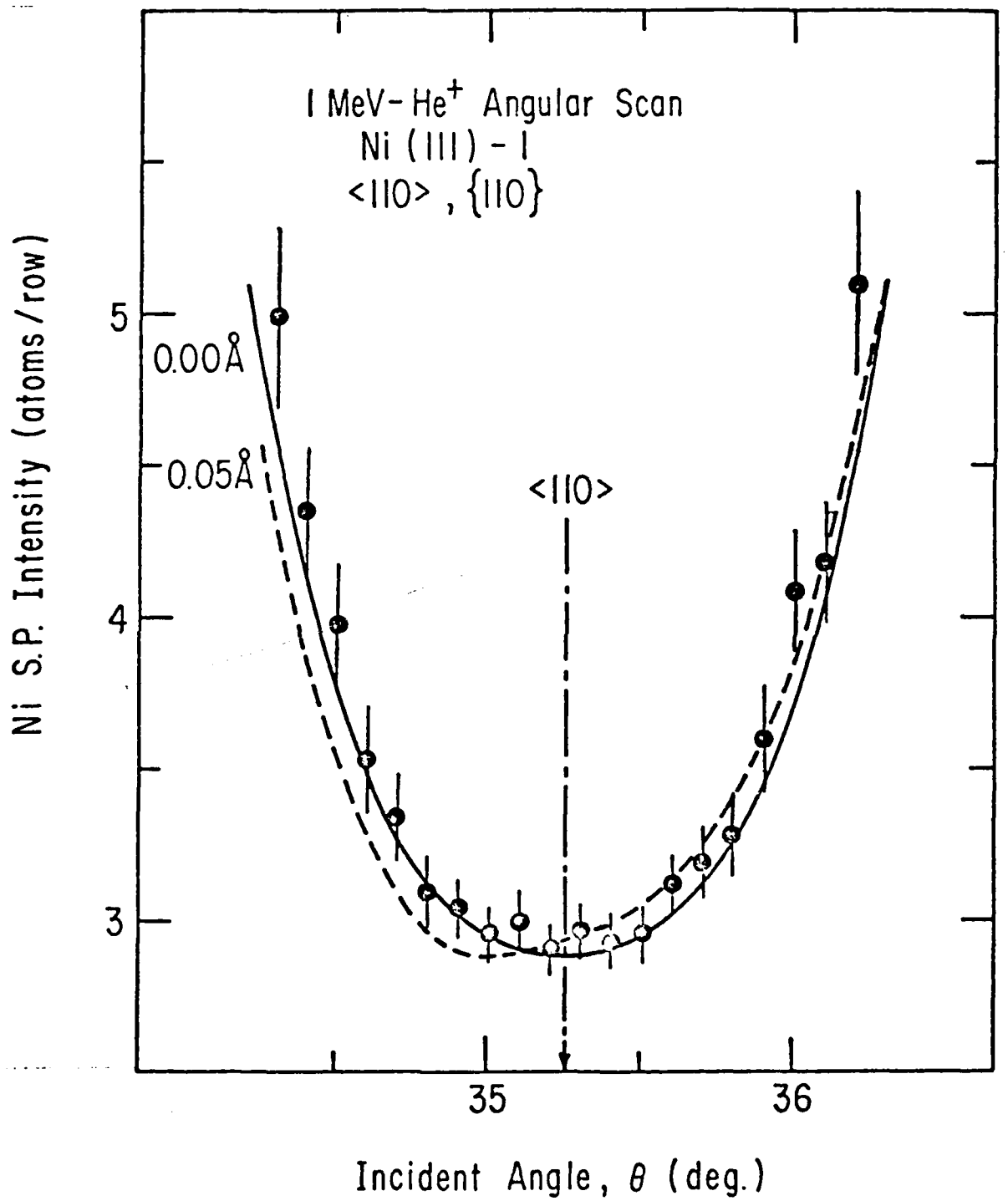
1 MeV-He+ Angular Scan
Ni (111) - 1
<110> , {110}
0.00Å
0.05Å
<110>
Ni S.P. Intensity (atoms/row)
5
4
3
35
36
Incident Angle, θ (deg.)

Fig. 5

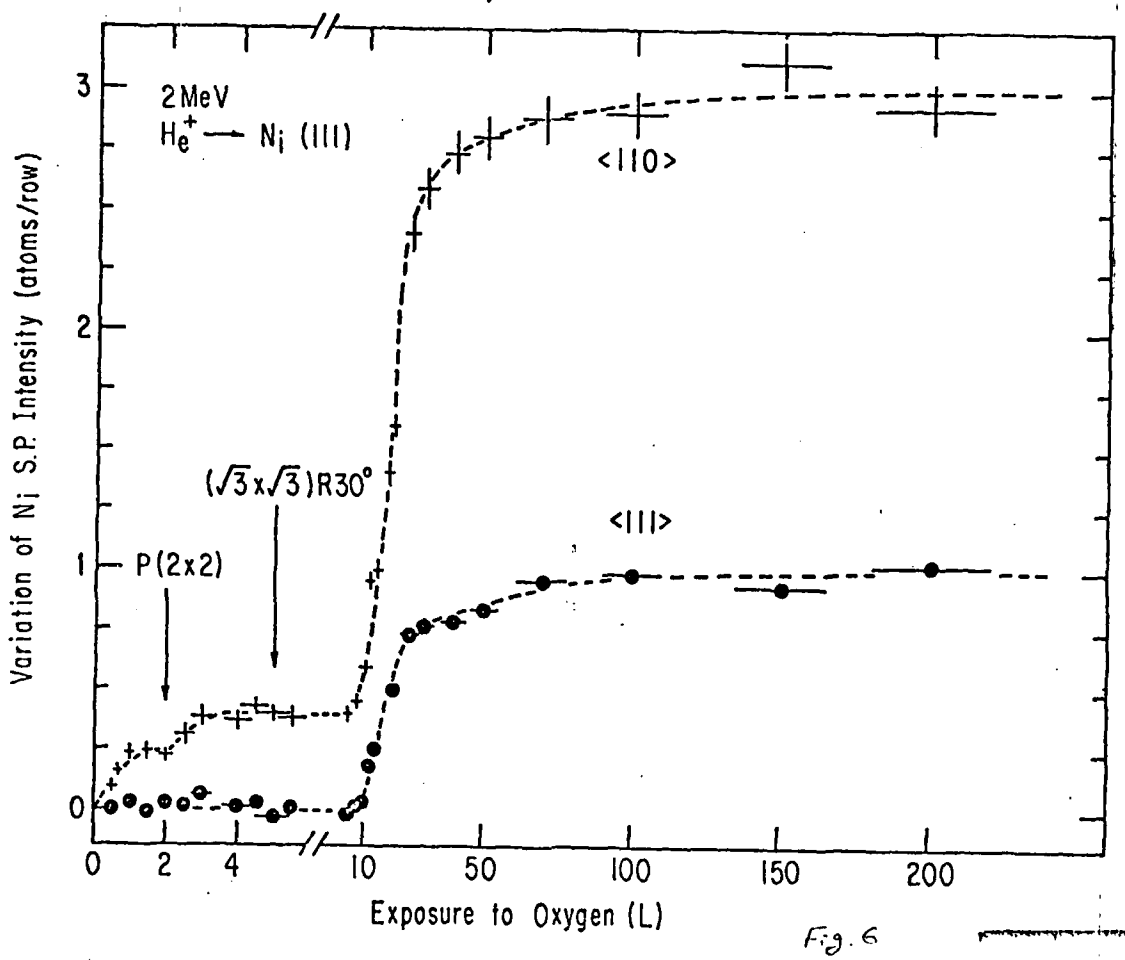
2MeV
$He^+ \rightarrow Ni$ (111)
<110>
<111>
$(\sqrt{3}x\sqrt{3})R30°$
P(2x2)
Variation of Ni S.P. Intensity (atoms/row)
Exposure to Oxygen (L)
0
1
2
3
0
2
4
10
50
100
150
200

Fig. 6

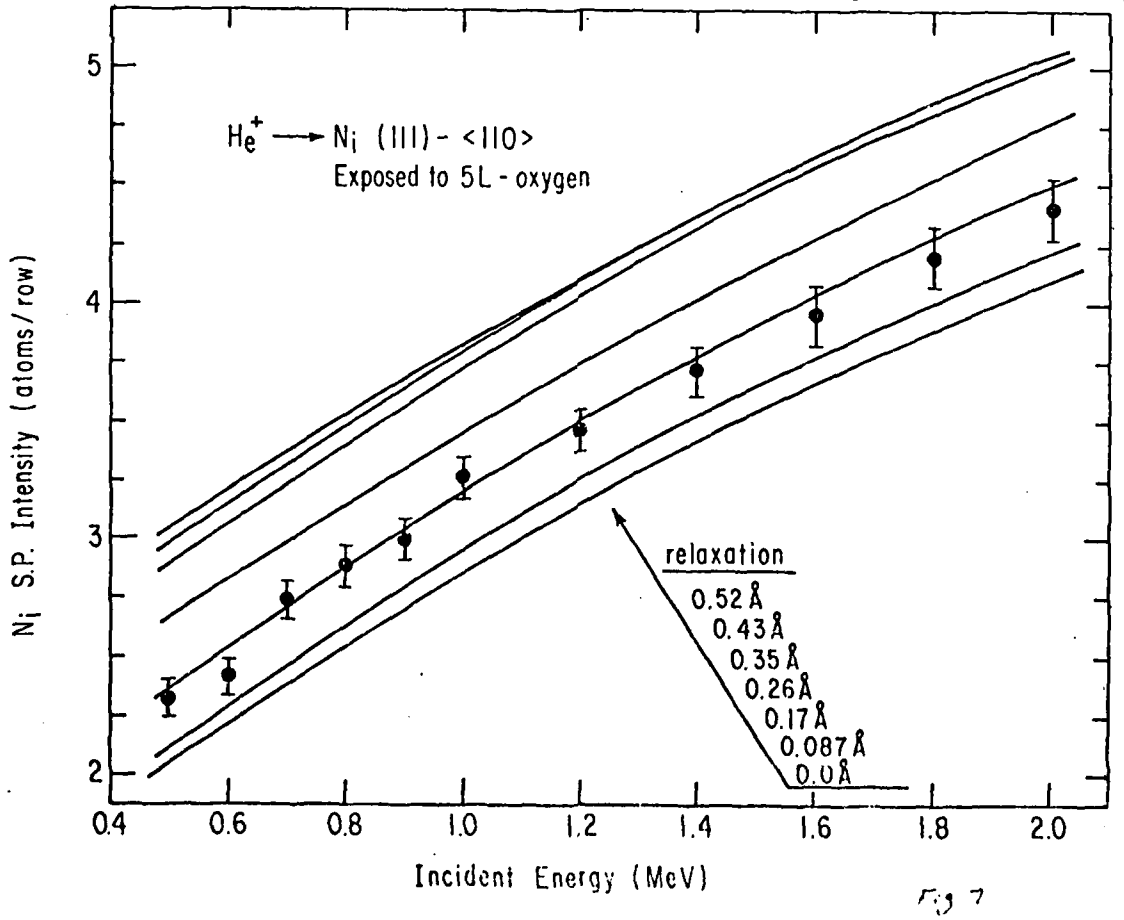
$He^+ \rightarrow Ni$ (111) - <110>
Exposed to 5L - oxygen
relaxation
0.52 Å
0.43 Å
0.35 Å
0.26 Å
0.17 Å
0.087 Å
0.0 Å
Ni S.P. Intensity (atoms/row)
Incident Energy (MeV)
2
3
4
5
0.4
0.6
0.8
1.0
1.2
1.4
1.6
1.8
2.0

Fig 7

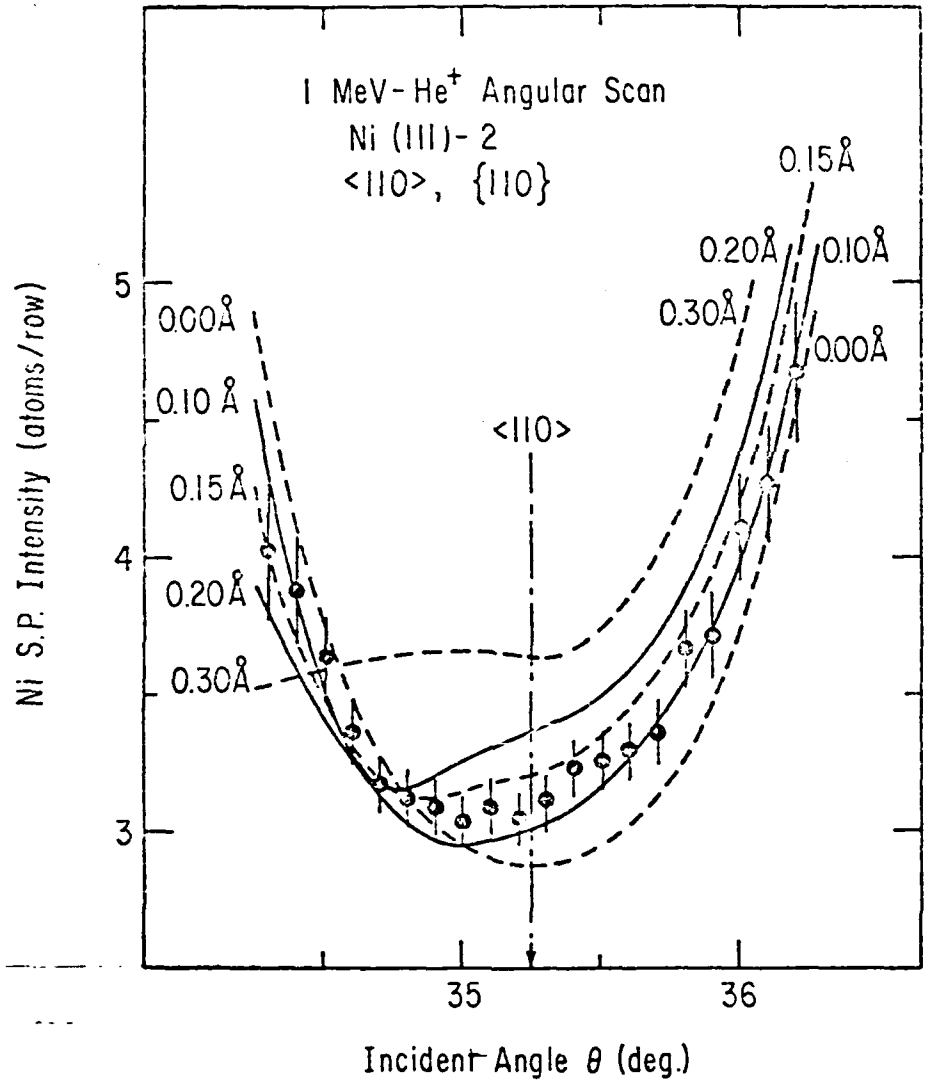
1 MeV-He+ Angular Scan
Ni (111)-2
<110>, {110}
0.15Å
0.20Å
0.10Å
0.30Å
0.00Å
0.00Å
0.10 Å
0.15Å
0.20Å
0.30Å
<110>
Ni S.P. Intensity (atoms/row)
5
4
3
35
36
Incident Angle θ (deg.)

Fig. 8(a)

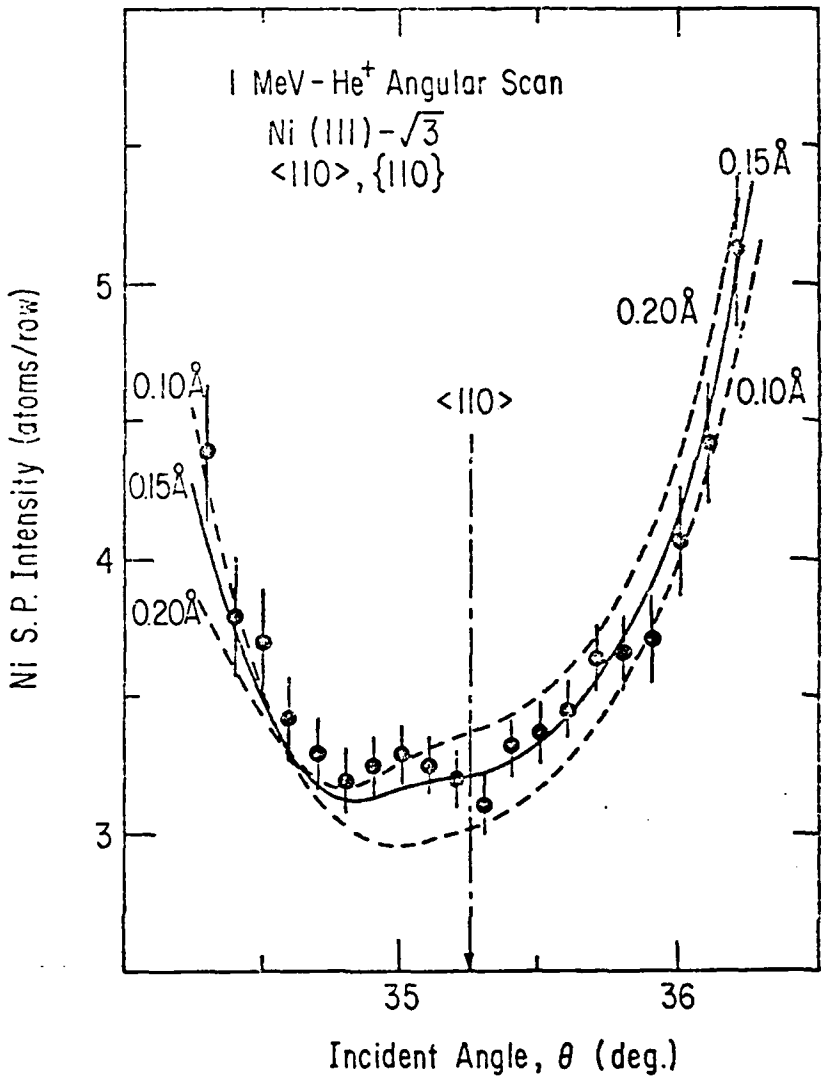
1 MeV-He+ Angular Scan
Ni (111)-√3
<110>, {110}
0.15Å
0.20Å
0.10Å
0.10Å
0.15Å
0.20Å
<110>
Ni S.P. Intensity (atoms/row)
5
4
3
35
36
Incident Angle, θ (deg.)

Fig. 8(b)

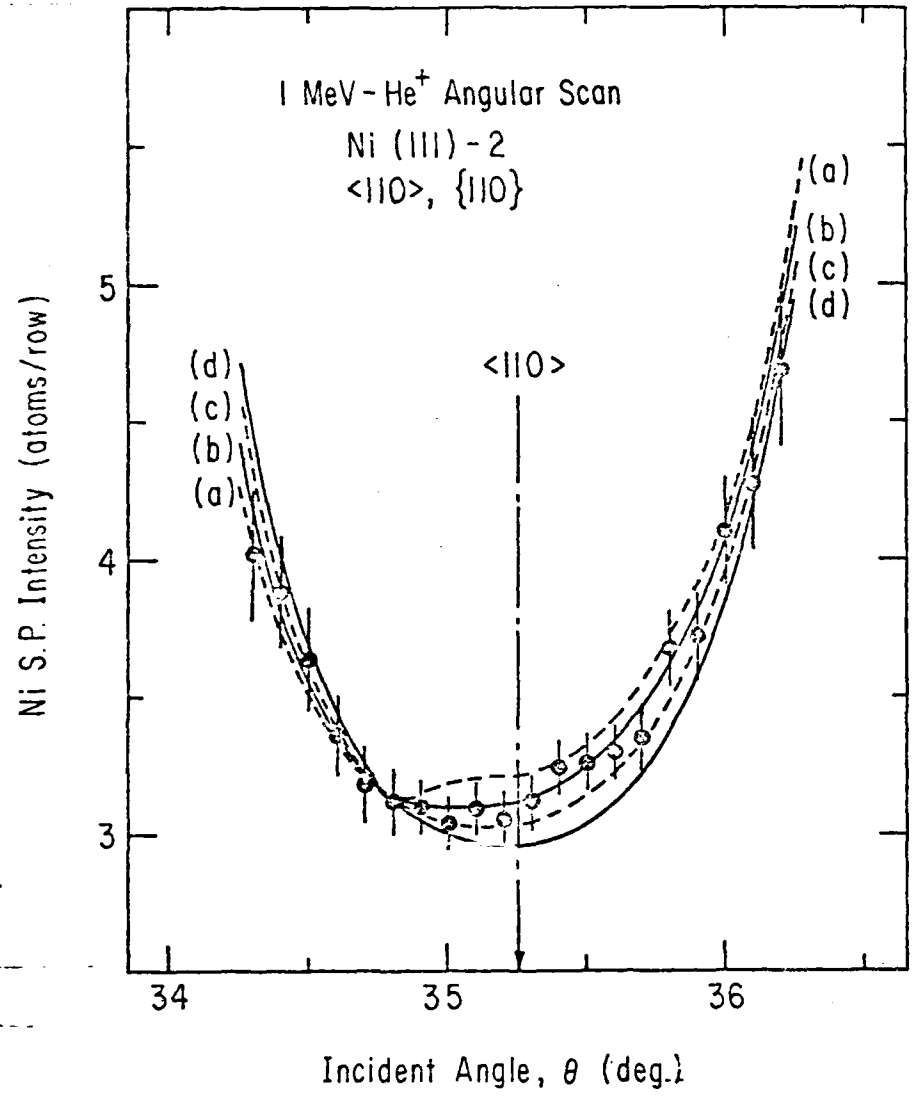
1 MeV - He+ Angular Scan
Ni (111) - 2
<110>, {110}
(a)
(b)
(c)
(d)
(d)
(c)
(b)
(a)
<110>
Ni S.P. Intensity (atoms/row)
5
4
3
34
35
36
Incident Angle, θ (deg.)

Fig. 9

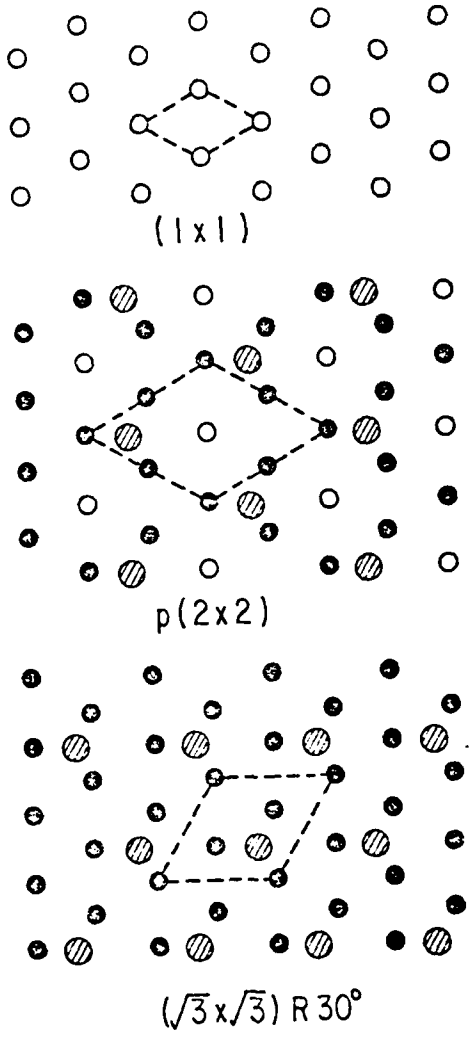
(1x1)
p(2x2)
(√3x√3) R 30°

Fig. 10

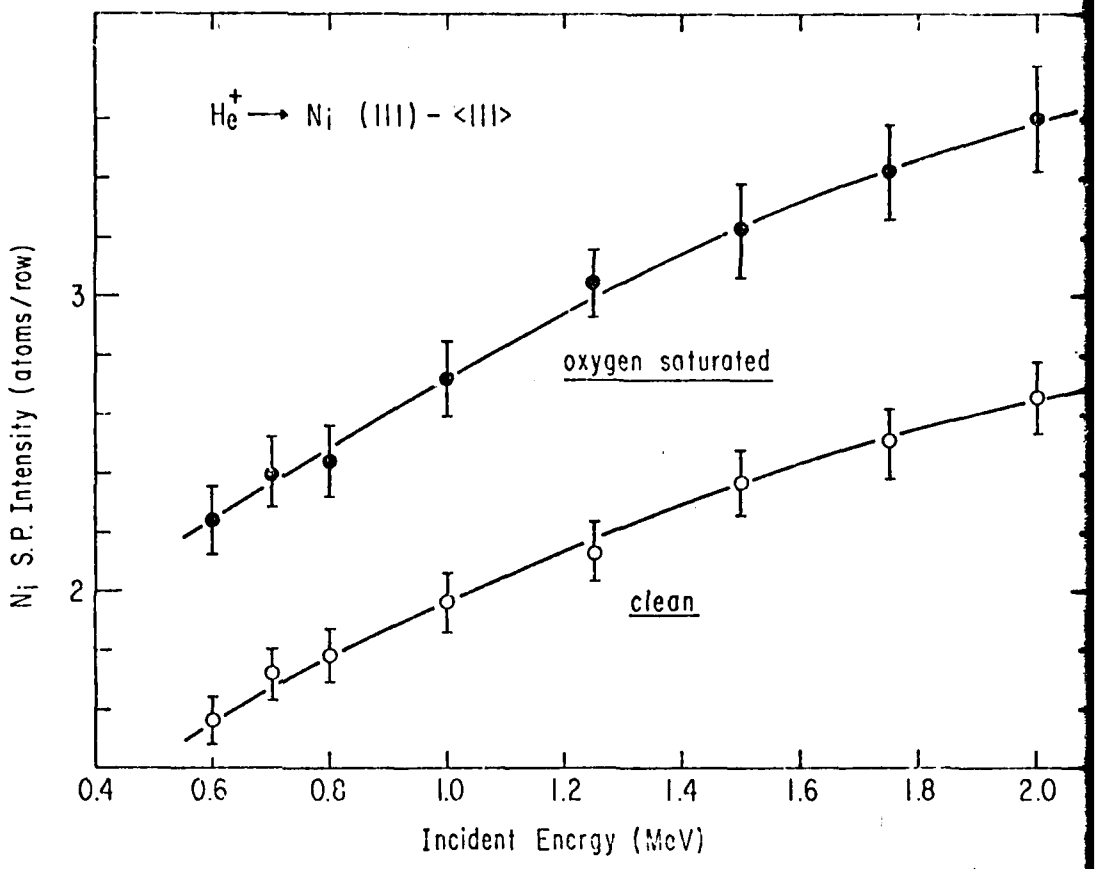

Fig. 11(a)

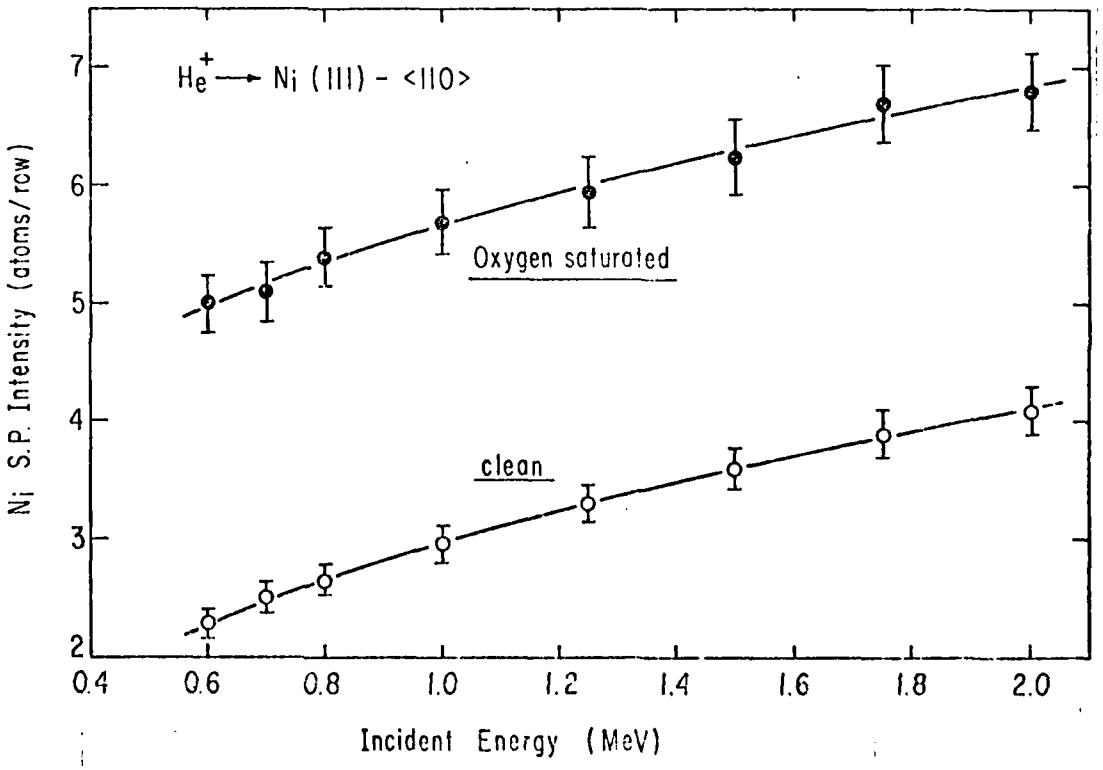

Fig. 11(b)

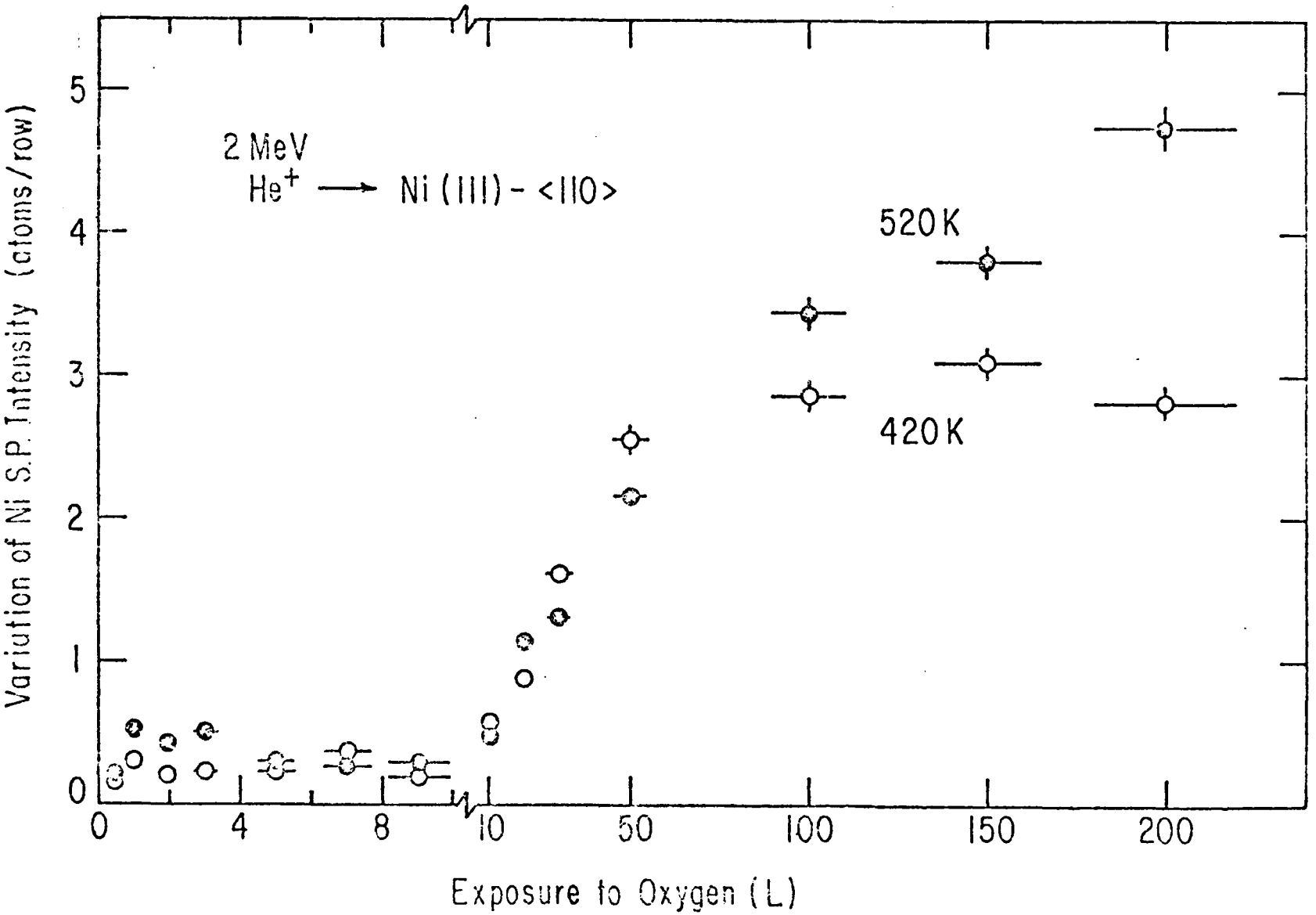
2 MeV
He+ → Ni (111) - <110>
520K
420K
Variation of Ni S.P. Intensity (atoms/row)
Exposure to Oxygen (L)
0
1
2
3
4
5
0
4
8
10
50
100
150
200

Fig. 12